Available online at www.sciencedirect.com
SCIENCE DIRECT®
Nuclear Instruments and Methods in Physics Research B 245 (2006) 511–518
NIM B
Beam Interactions with Materials & Atoms
www.elsevier.com/locate/nimb

Micro-PIXE characterization of interactions between a sol–gel derived bioactive glass and biological fluids

J. Lao [a,*], J.M. Nedelec [b], Ph. Moretto [c], E. Jallot [a]

[a] Laboratoire de Physique Corpusculaire de Clermont-Ferrand, CNRS/IN2P3 UMR 6533, Université Blaise Pascal, 24 avenue des Landais, 63177 Aubière Cedex, France
[b] Laboratoire des Matériaux Inorganiques, CNRS UMR 6002, Université Blaise Pascal, 24 avenue des Landais, 63177 Aubière Cedex, France
[c] Centre d'Etudes Nucléaires de Bordeaux Gradignan, CNRS/IN2P3 UMR 5797, Université Bordeaux 1, Chemin du Solarium, Le Haut-Vigneau, BP 120, 33175 Gradignan Cedex, France

Received 27 October 2005
Available online 28 February 2006

Abstract

Bioactive glasses possess the ability to bond to living tissues through the formation of a calcium phosphate-rich layer at their interface with living tissues. This paper reports the different steps of this bioactivity process via a complete micro-PIXE characterization of a sol–gel derived SiO_2–CaO bioactive glass in contact with biological fluids for different delays. Multi-elemental cartography at the glass/biological fluids interface together with major and trace elements quantification permit a better understanding of the five reaction stages involved in the bioactivity mechanisms. The presence of phosphorus was detected at the periphery of the material within 6 h of interaction with biological fluids. A calcium phosphate-rich layer containing magnesium is formed after a few days of interaction and presence of bone-like apatite is deduced from the calculation of the Ca/P ratio at the material interface. That is of deep interest for clinical applications, because this biologically active behavior results in the formation of a strong interfacial bond between the glass and host tissues, and will stimulate bone–cell proliferation.

PACS: 68.08.−p; 81.05.Kf; 81.20.Fw; 82.80.Ej; 82.80.Yc; 87.64.Gb; 87.68.+z

Keywords: PIXE–RBS methods; Biomaterials; Bioactive glass; Sol–gel

1. Introduction

Bioactive materials have been developed to preserve the comfort of living of people suffering from functional deficiency. They are widely used in surgical therapeutics for filling bony defects, solving cardiovascular and articular problems, repairing conductive hearing loss and in a growing number of clinical applications [1]. In contact with body fluids, bioactive materials induce a specific biological response at their surface which permits an intimate bonding to living tissues [2]. Due to a series of physico-chemical reactions occurring at the surface of the material, the bone-bonding ability consists to the formation of a carbonate-containing hydroxyapatite ($Ca_{10}(PO_4)_6(OH)_{2(1-x)}(CO_3)_x$) layer similar to the mineral composition of bone [3]. This property is known as bioactivity.

When put in contact with tissues, biological glasses show biocompatibility and absence of inflammatory response. They can be bioinert or bioactive depending on their composition and their textural properties. Dissolution of calcium and silicate ions from glasses plays an important role in forming the apatite layer [4]. The recognition that the material textural properties are a critical element for the formation of the bonding bone-like apatite layer is a major argument to use the sol–gel process. It permits the synthesis of a bioactive glass with an initial high specific

* Corresponding author. Tel.: +33 (0)4 73 40 76 51; fax: +33 (0)4 73 26 45 98.
E-mail address: lao@clermont.in2p3.fr (J. Lao).

0168-583X/$ - see front matter © 2005 Elsevier B.V. All rights reserved.
doi:10.1016/j.nimb.2005.12.049

surface area [5]. Further motivations for sol–gel processing are the potentially higher purity and homogeneity, the lower processing temperatures associated with sol–gel derived materials compared with traditional glass melting or ceramic powder methods and the relative economics of sol–gel methods in general [6]. Another strong advantage of the sol–gel process is the possibility to produce materials in various shapes such as monoliths, powders, fibers or coatings.

Sol–gel glasses in the SiO_2–CaO system have been proved to form a calcium phosphate-rich layer at their surface. The initially amorphous calcium phosphate then crystallizes into an apatite analogous to that present in bone. The apatite crystals, reinforced by collagen fibers, form the bonding layer between the bioactive material and the living tissues [7]. The aim of this paper is to report the synthesis of a SiO_2–CaO bioactive glass by sol–gel processing and to characterize the acellular in vitro development of the calcium phosphate-rich layer on its surface during interactions with biological fluids. For this purpose, bioactive glass samples were immersed in biological fluids for varying time periods. Knowledge of the elemental distribution at the bioactive glass periphery is important to understand the physico-chemical mechanisms that lead to the formation of a calcium phosphate layer [8]. This analysis was performed by particle-induced X-ray emission (PIXE) and Rutherford backscattering spectroscopy (RBS). These ion beam analysis methods allow us to measure the elemental composition of the glass immersed samples at the micrometer scale and to obtain elemental maps together with major and trace elements quantification.

2. Materials and methods

2.1. Preparation of the bioactive glass samples

Gel-glass powders containing 75wt%SiO_2–25wt%CaO were prepared using the sol–gel process. Low-viscosity sol was obtained by mixing tetraethylorthosilicate (TEOS) and $Ca(NO_3)_2 \cdot 4H_2O$ in ethanol EtOH, 99%. Deionised water was added with a water to alkoxide ratio equal to 12. 2 N HCl was used as a catalyst for the hydrolysis of TEOS. The prepared sol was then transferred to an oven at 60 °C for gelation. Four hours later, the gelation began and the obtained gel was dried at 125 °C for 24 h. At this time, the xerogel appears as a white powder and is finally heated at 700 °C for 24 h to achieve nitrate elimination and further densification. The dry gel powder was then compacted into discs of 13 mm diameter and 2 mm height.

2.2. Material characterization

We used inductively coupled plasma-atomic emission spectroscopy (ICP-AES) to determine the chemical composition of the bioactive glass powder. The nominal and experimental glass compositions are presented in Table 1.

Table 1
Nominal and experimental concentrations (wt%) of Si and Ca oxides in the glass powder

	Nominal	Experimental
SiO_2 (wt%)	75	72.20 ± 0.37
CaO (wt%)	25	24.50 ± 0.17

The textural characterization of the samples was performed on a Coulter SA 3100 gas sorption system. The sample was vacuum outgassed at 120 °C for 12 h to remove physically adsorbed molecules such as moisture from the pores, and analyzed with nitrogen adsorption and desorption. The instrument determined isotherms volumetrically by a discontinuous static method at 77 K. The surface area was obtained by applying the BET method [9] to the N_2 isotherm. The pore size distribution was determined by the BJH method [10] on the desorption branch. Total pore volume was measured at a relative pressure $P/P_0 = 0.99$.

2.3. In vitro studies

The glass discs were immersed at 37 °C for 1, 6 h and 1, 2, 5, 10 d in 45 mL of a standard Dulbecco's modified eagle medium (DMEM, Biochrom AG, Germany), which composition is almost equal to human plasma. After interaction, the discs were removed from the fluid, air dried and embedded in resin (AGAR, Essex, England). Before characterization, thin sections of 30 μm nominal thickness were prepared using a Leica RM 2145 microtome. Cutting is made perpendicular to the surface of the glass discs. Then, the sections are placed on a mylar film with a hole of 3 mm in the centre. Measurements are performed on the area of the section placed over the hole.

2.4. PIXE–RBS analysis

PIXE and RBS methods are used simultaneously. The PIXE method permits to identify and to quantify locally major and trace elements at the biomaterial/biological fluids interface. The RBS method is used to determine the electric charge received by the samples during irradiation. This parameter is absolutely necessary for PIXE spectra quantification [11].

Analyses of the biomaterial/biological fluids interface were performed using nuclear microprobes at CENBG (Centre d'Etudes Nucléaires de Bordeaux – Gradignan, France). The device provides a micro-beam line employed for ion beam analytical measurements at the microscopic level. The experimental characteristics of the CENBG nuclear microprobe have been published previously [12]. For PIXE analyses, we chose proton scanning micro-beam of 1.5 MeV energy and 100 pA in intensity to ionize atoms of the glass samples. The beam diameter was nearly 2 μm. Such parameter values are justified by a higher ionization cross-sections of light elements ($Z < 20$) and a better sensitivity resulting for PIXE analysis by using a detector without filter. Furthermore, weak intensity and the choice of

protons as the ion beam allow the target degradation to be minimized during irradiation. However, the intensity is not too weak and permits measurement duration under 1 h.

An 80 mm^2 Si(Li) detector was used for X-ray detection. The Si(Li) semiconductor was orientated at 135° with respect to the incident beam axis and equipped with a beryllium window 12 μm thick. PIXE spectra are treated with the software package GUPIX, developed at Guelph University, Canada [13]. GUPIX determines the intensities of characteristic X-ray peaks in a PIXE spectrum by fitting a model spectrum to the measured one using the nonlinear least squares technique, together with subsequent conversions of the fitted X-ray peak intensities to elemental concentrations via defined standardization technique (involving solid angle of detection, relative charge and user-determined instrumental constants).

Relating to RBS, a silicon particle detector placed 135° from the incident beam axis allowed us to monitor the total number of protons that interacted with the sample via the yield of backscattered particles. Data were treated with the SIMNRA code developed at the Max-Planck-Institut für Plasma Physik, Germany [14].

3. Results

3.1. Characterization of the glass powder before the in vitro assays

Thanks to sol–gel processing, bioactive glass powders were obtained with a good agreement between nominal and experimental concentrations of Ca and Si oxides determined by ICP-AES (Table 1). The textural properties are summarized in Table 2. The synthesized SiO_2–CaO glass is a mesoporous material, with a modal pore diameter of 71.4 Å (calculated by the BJH method). That is typical of sol–gel derived materials. Such textural characteristics will have major effects on the material dissolution and kinetics of physico-chemical reactions at its surface, and thus influence the bioactivity process and the calcium phosphate-rich layer formation.

3.2. Evaluation of irradiation damages

Micro-beam can cause target degradation [15]. These damages induce mass losses, which will affect the elemental concentration determinations. Scanning micro-beam protects sample only if the amount of deposited charge is small [16]. Verifying the behavior of our samples under irradiation is thus essential to be ensured of the accuracy of the measured concentrations. We irradiated a sample of the primary synthesized SiO_2–CaO bioactive glass for 1 h. By examination of the RBS data, we determined the total electric charge deposited. We finally obtained Si and Ca concentrations in the sample with intervals of regular times that are equivalent with percentage of the total deposited charge (Fig. 1). Our samples are relatively stable during irradiation. When the samples are irradiated, part of oxygen and hydrogen volatilizes, causing matrix calculation to be distorted. This phenomenon explains the fluctuations in the elemental concentration determination, which are in the order of 5%.

Table 2
Textural properties of the SiO_2–CaO glass powder

	SiO_2–CaO glass powder
Surface area	26 m^2/g
Pore volume	0.94 cm^3/g
Modal pore diameter	71.4 Å

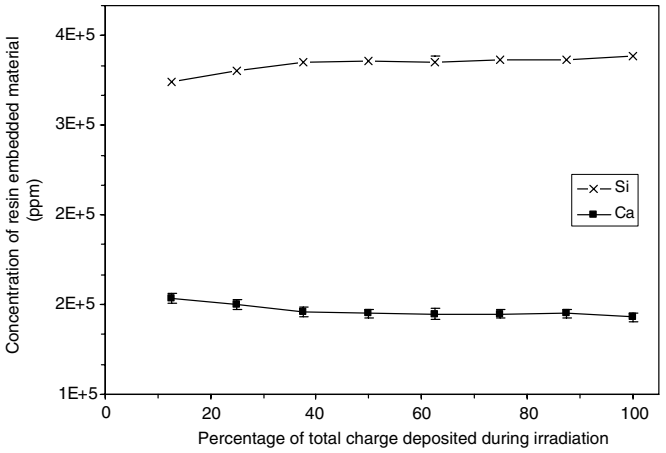

Fig. 1. Si and Ca concentrations (ppm) in the synthesized SiO_2–CaO glass versus deposited charge during irradiation (%).

3.3. Micro-PIXE study of the discs

The PIXE method permits elemental cartography at the micrometer level. Elemental maps across the periphery of the SiO_2–CaO glass were recorded for each immersion time in DMEM. Then, quantification of major and trace elements was performed by mean of GUPIX.

In Fig. 2, we present multi-elemental maps across the periphery of the primary SiO_2–CaO glass before immersion into DMEM. We detect the initial elements (Si, Ca) of the glass and Cl, which is a resin component. On the maps, we clearly observe two zones. The first area is composed with Si, Ca and represents the bioactive glass. The second is composed with Cl and shows the presence of resin at the surface of the glass disc. The glass disc has a homogeneous composition. On both Si and Ca maps, we can note the presence of white areas in the glass, indicating that the section is locally torn.

After 1 h of interaction, the presence of P is detected at the periphery of the glass, as well as low concentration of Mg (data not shown). Concerning Si and Ca, a gradient of concentration is observed from the periphery of the material to the centre of the glass disc.

Fig. 3 shows the multi-elemental maps of a disc sample after 6 h of interaction with biological fluids. We observe two areas at bioactive glass disc surface. The first area is

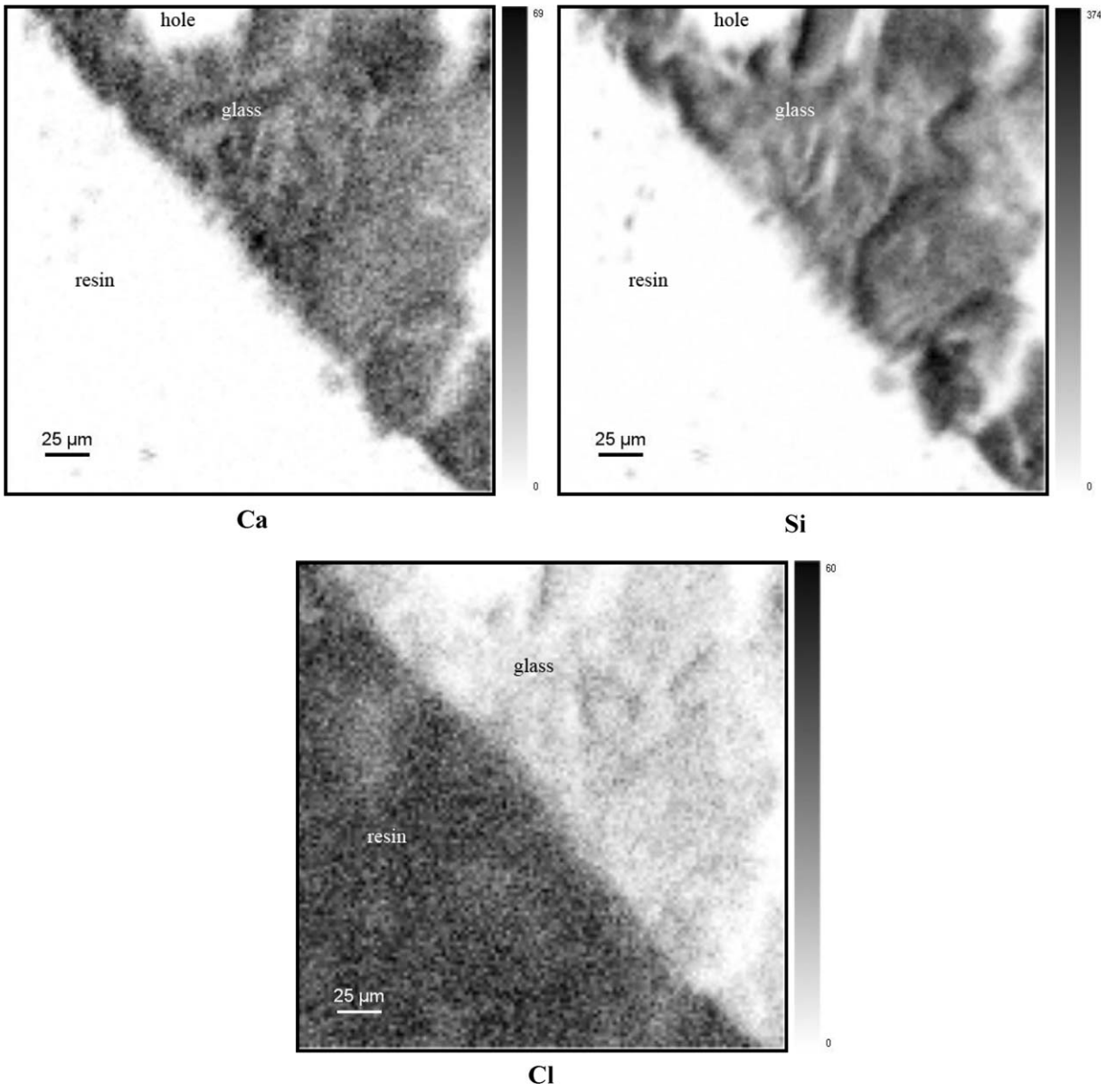

Fig. 2. Si, Ca and Cl maps across the periphery of the synthesized SiO_2–CaO glass before the in vitro assays (275×275 μm^2).

composed with Si, Ca and represents the glass in dissolution. The second area is at the surface of the glass and is essentially composed with Si, Ca and P together with traces of Mg. The thickness of this layer is about 10 μm. It clearly appears that the glass is in dissolution, as Ca is removed from the network. After 10 d of interaction with biological fluids (Fig. 4), three areas appear. The inner glass consists of the primary silicate network enduring dissolution. A homogeneous calcium phosphate-rich layer is formed at the material surface. This layer contains Mg and its thickness is in the order of 15 μm. Between those areas, we observe the presence of a thin calcium-enriched layer.

Thus, we examined variations relative to immersion time of Si, Ca, P and Mg concentrations at both the material periphery (Fig. 5) and within the glass disc (Fig. 6). At the periphery of the glass, Ca concentration decreases by 30% during the first 6 h of soaking (Fig. 5). Despite some variations, Si concentration tends to decrease during this time period. P is blended into the material in an obvious way, since its concentration increases up to 44,000 ppm after 6 h of immersion. The local increase of phosphorus concentration is highlighted in Fig. 3. Between 6 h and 2 d of soaking, Ca and P concentrations roughly increase. On the contrary, Si concentration significantly decreases. These concentrations continue to increase with time of exposure to DMEM and after 10 d of immersion, the phosphorus amount at the glass periphery reaches up to 12 wt%. Concerning Mg, it appears after 1 h of immersion and its concentration remains almost the same during

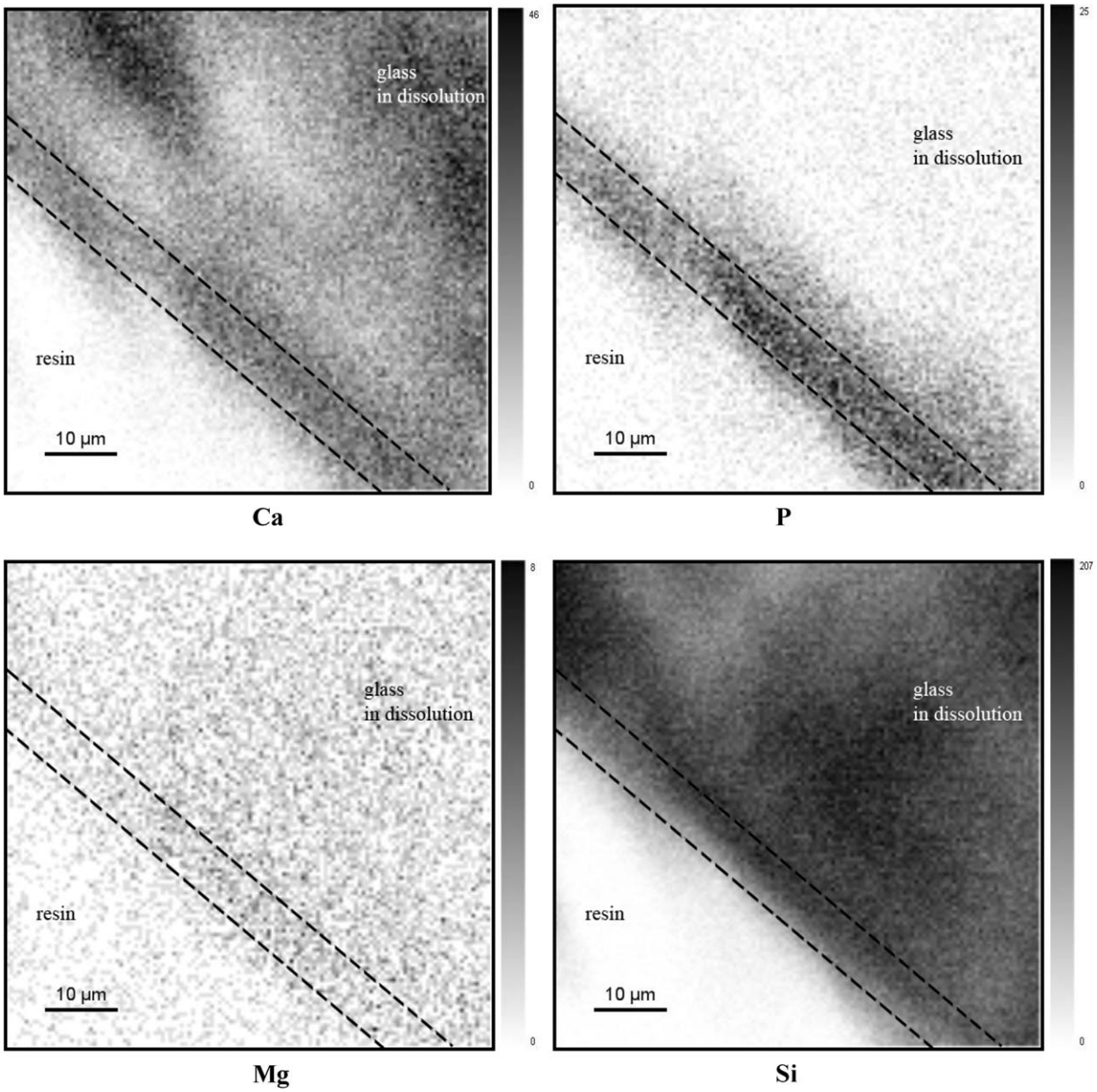

Fig. 3. Si, Ca, P, Mg maps of the SiO_2–CaO glass after 6 h of immersion in DMEM (67×67 μm^2).

the assays. This element was incorporated with the calcium phosphate-rich layer as a trace element (as visible in Fig. 4).

In the inner glass, Si and Ca showed totally opposed behaviors (Fig. 6). Between 1 h and 2 d, certain fluctuations in the values of Si and Ca concentrations were observed. P and Mg concentrations are low. They evolved in the same way, reaching a peak value after 1 d of exposure. After 2 d, both Si and Ca concentrations gradually returned to their initial values, while P and Mg concentrations were almost null.

Fig. 7 shows the evolution of the Ca/P atomic ratio at the periphery of the glass (Ca–P layer) for each immersion time. The Ca/P atomic ratio progressively decreases and remains equal to 2.0 after 5 d. This result shall be confronted to the Ca/P nominal value of pure hydroxyapatite, which is equal to 1.7.

4. Discussion

4.1. Physico-chemical reactions at the bioactive glass surface

In this work, we study surface changes of sol–gel derived bioactive glass discs in the SiO_2–CaO system and soaked in a biological solution. To better understand mechanisms of interaction between the bioactive glass and biological fluids a physico-chemical approach is used, namely the characterization of the modification kinetics of the discs periphery by means of PIXE–RBS methods. Micro-PIXE associated

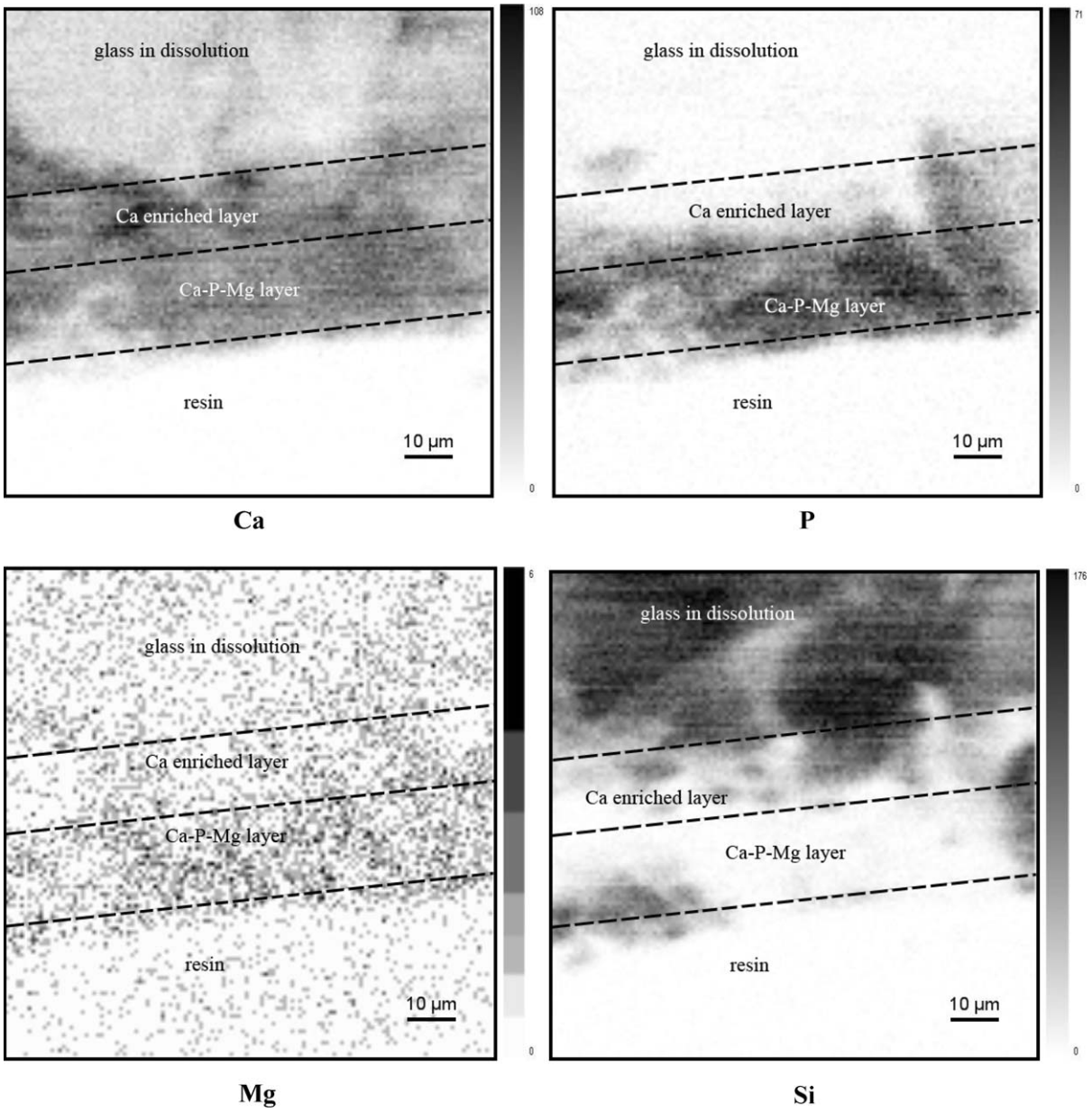

Fig. 4. Si, Ca, P, Mg maps of the SiO_2–CaO glass after 10 d of immersion in DMEM (99×99 μm^2).

to RBS allow us to obtain quantitative elemental maps of all elements with $Z > 11$ at the micrometer scale. Thanks to PIXE method, we are able to study major, minor and even trace elements (like Mg) with concentrations of a few ppm. After different delays of immersion in biological fluids, chemical maps across the periphery of glass discs show the physico-chemical reactions occurring at the surface of the glass disc.

During interactions between bioactive glass discs and biological fluids, the glass composition evolves with time of immersion. The different steps of bioactivity mechanism are visible in Figs. 5 and 6. Ca concentration decreases during the first 6 h. Si concentration at the periphery of the glass decreases by 10% after 1 h of interaction (loss of soluble silica to the solution). However, a silica-rich layer seems to be formed at the surface within 6 h. At this time period, P and Mg are detected as trace elements at the surface of the glass. In the inner glass, Si and Ca concentrations evolve in an opposite way because Si and Ca oxides content represent nearly 100% of the glass. Fluctuations in Si and Ca concentrations during the first 2 d are explained by the deep structural changes occurring in the glass network, as well as dealkalization and calcium migration process leading to the appearance of a locally calcium-enriched layer. Fig. 3 shows those changes, as well as the amorphous calcium phosphate layer formation concurrently beginning. Growth of this layer is proved by the significant increase of Ca and P concentrations at the glass surface. Finally, we obtain a multilayer material with the formation of a Ca-rich layer and a Ca–P-rich layer (Fig. 4). Presence of Mg is detected in the calcium phosphate layer. Mg can play an important role during

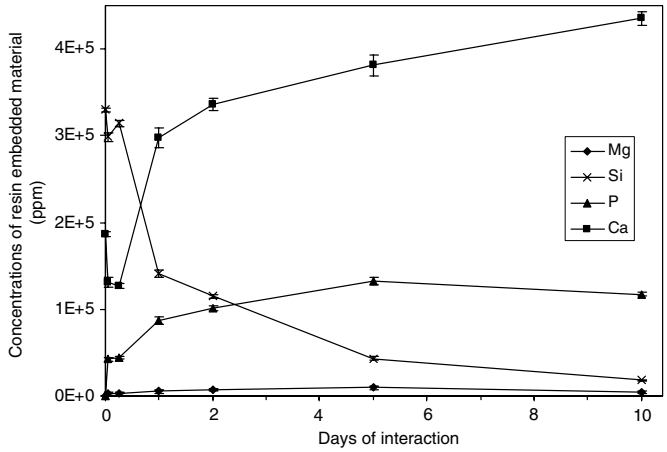

Fig. 5. Evolution of Ca, P, Mg and Si concentrations (ppm) at the glass periphery with time of exposure to DMEM.

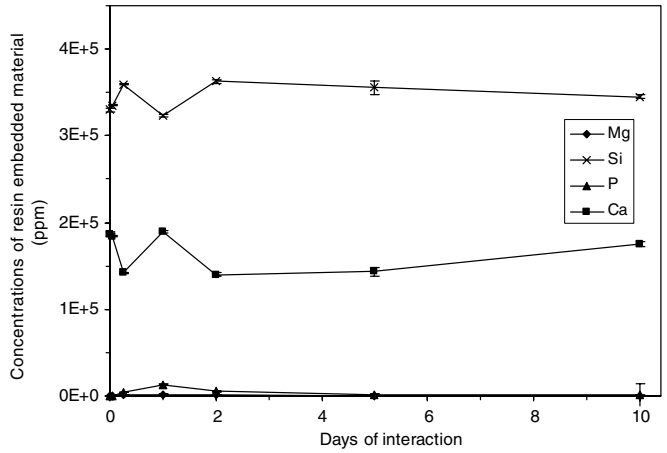

Fig. 6. Evolution of Ca, P, Mg and Si concentrations (ppm) within the glass with time of exposure to DMEM.

spontaneous formation of in vivo calcium phosphates and bone bonding [17,18].

The basis of bone-bonding property of bioactive glasses is the chemical reactivity of the material in contact with biological fluids [19]. The formation of the apatite layer occurs through physico-chemical reactions which can be decomposed into five steps [20,21]. The first stage is the dealkalization of the surface by rapid exchange of Ca^{2+} cations with H^+ from solution. Hence, Ca concentration in the material decreased during the first 6 h of exposure to DMEM. This reaction is immediately followed by a breakdown of the silica network enduring dissolution, forming silanol bonds at the glass interface (second stage) that repolymerize to form a hydrated, high surface-area, silica-rich layer (third stage). This silica-rich surface attracts organic molecules and facilitates the formation of the apatite layer on the glass. Indeed, the fourth reaction stage is the migration of Ca^{2+} groups from the glass to the surface through the SiO_2-rich layer, followed by growth of the amorphous calcium phosphate-rich film by incorporation of soluble calcium and phosphates from solution. Finally, the fifth reaction stage consists of the crystallization of the amorphous calcium phosphate by incorporation of OH^-, CO_3^{2-} anions and Mg^{2+} cations from solution to form an apatite layer.

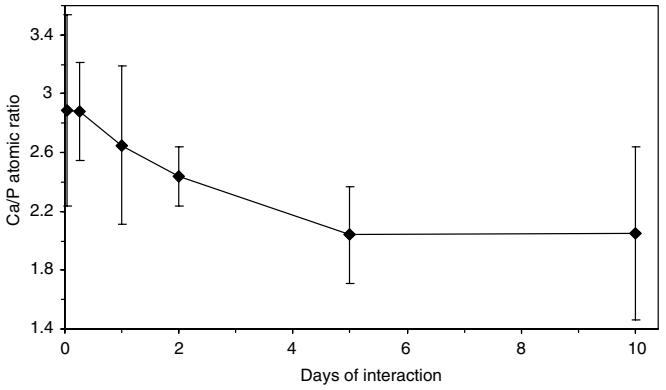

Fig. 7. Ca/P atomic ratio in the Ca–P layer versus time of exposure to DMEM.

The Ca–P layer formation (fifth stage) might be deduced from Fig. 7. After 5 d, the Ca/P atomic ratio at the glass interface remains equal to 2.0, which is near the characteristic apatite value of 1.7. This variation might be explained by the mechanism of apatite formation. The elements concentrations for the Ca/P ratio calculation were determined across the CaP-rich layer. However the crystallization of the amorphous calcium phosphate takes place on particular favorable sites for apatite nucleation, leading to the formation of an apatite-like phase consisting of small crystallites of estimated size 140 Å [7,22,23]. Therefore, the Ca/P ratio calculation is distorted by the presence of amorphous calcium phosphate locally subsisting between nucleation sites. In addition, Mg^{2+} can substitute into the apatite lattice, causing its physico-chemical properties to change. In fact, apatite substituted with Mg results in a Ca deficient apatite with lower crystallinity and higher solubility [24,25].

5. Conclusion

The results of the present work showed that the SiO_2–CaO glass is able to induce the formation of an apatite layer, indicating that it is bioactive. Micro-analysis with the PIXE method allowed us to specify the role of major elements (Si, Ca, P) and trace elements (Mg) in the physico-chemical reactions occurring at the periphery of the glass. Moreover, explicit multi-elemental maps were obtained, highlighting the calcium phosphate-rich layer formation and the evolution of the glass network.

The reason for choosing a glass in the SiO_2–CaO binary system was first a higher homogeneity in the glass to be expected. Furthermore, the study of the Ca–P layer growth process was easier since the phosphate ions were only coming from the solution. The calcium phosphate-rich layer containing magnesium was quickly formed, following five

reaction stages. It is important to notice that this layer grows up in an acellular environment and therefore its spontaneous formation was only due to the SiO_2–CaO bioactive properties. The formation of biologically active apatite layer is a prerequisite to bond to host tissues.

References

[1] L.L. Hench, J. Am. Ceram. Soc. 74 (1991) 1487.
[2] L.L. Hench, J.K. West, Life Chem. Rep. 13 (1996) 187.
[3] L.L. Hench, R. Splinter, W. Allen, T. Greenlee, J. Biomed. Mater. Res. 2 (1971) 117.
[4] T. Kokubo, Biomaterials 12 (1991) 155.
[5] R. Li, A.E. Clark, L.L. Hench, J. Appl. Biomater. 2 (1991) 231.
[6] L.L. Hench, J.K. West, Chem. Rev. 90 (1990) 33.
[7] I. Izquierdo-Barba, A.J. Salinas, M. Vallet-Regí, J. Biomed. Mater. Res. 47 (1999) 243.
[8] E. Jallot, in: H.S. Nalwa (Ed.), Encyclopedia of Nanoscience and Nanotechnology, Vol. 7, American Scientific Publishers, 2004, p. 405.
[9] S. Brunauer, P.H. Emmet, E. Teller, J. Am. Chem. Soc. 60 (1938) 309.
[10] E.P. Barret, L.G. Joyner, P.P. Halenda, J. Am. Chem. Soc. 73 (1951) 373.
[11] Y. Barbotteau, J.L. Irigaray, E. Jallot, Surf. Interface Anal. 35 (2003) 450.
[12] Y. Llabador, P. Moretto, H. Guegan, Nucl. Instr. and Meth. B 77 (1993) 123.
[13] J.A. Maxwell, W.J. Teesdale, J.L. Campbell, Nucl. Instr. and Meth. B 95 (1995) 407.
[14] M. Mayer, Nucl. Instr. and Meth. B 194 (2002) 177.
[15] B.J. Kirby, G.J.F. Legge, Nucl. Instr. and Meth. B 54 (1991) 98.
[16] M. Cholewa, G. Bench, B.J. Kirby, G.J.F. Legge, Nucl. Instr. and Meth. B 54 (1991) 101.
[17] E. Jallot, Appl. Surf. Sci. 211 (2003) 89.
[18] E. Jallot, J.M. Nedelec, A.S. Grimault, E. Chassot, A. Grandjean-Laquerrière, P. Laquerrière, D. Laurent-Maquin, Colloids Surf. B 42 (2005) 205.
[19] P. Saravanapavan, J.R. Jones, R.S. Pryce, L.L. Hench, J. Biomed. Mater. Res. A 66 (2003) 110.
[20] J. Zhong, D.C. Greenspan, J. Biomed. Mater. Res. B 53 (2000) 694.
[21] E. Jallot, H. Benhayoune, L. Kilian, Y. Josset, Langmuir 19 (2003) 3840.
[22] T. Kokubo, H. Kushitani, S. Sakka, J. Biomed. Mater. Res. 24 (1990) 721.
[23] C. Ohtsuki, T. Kokubo, T. Yamamuro, J. Noncryst. Solids 143 (1992) 84.
[24] R.Z. Legeros, R. Kijkowska, I. Kattech, M. Jemal, J.P. Legeros, J. Dent. Res. 65 (1983) 783.
[25] M. Vallet-Regí, A.J. Salinas, J. Román, M. Gil, J. Mater. Chem. 9 (1999) 515.